Journal of Bionic Engineering
https://doi.org/10.1007/s42235-021-00150-4

RESEARCH ARTICLE

Computational Design and Fabrication of a Bending-Active Structure Using Fiberglass: A Bioinspired Pavilion Mimicking Marine Microorganism Radiolaria

Bosheng Liu[1] · **Tanvir R. Faisal**[2]

Received: 21 April 2021 / Revised: 8 December 2021 / Accepted: 13 December 2021
© Jilin University 2022

Abstract
Bio-inspired architectural designs are often superior for their aesthetics and structural performance. Mimicking forms and loading states of a biological structure is complex as it requires a delicate balance among geometry, material properties, and interacting forces. The goal of this work is to design a biomimetic, ultra-lightweight, bending-active structure utilizing an informed integral design approach, and thereby constructing a self-supporting cellular pavilion. A bioinspired pavilion has been designed and constructed based on the natural cellular organization observed in Radiolaria, a deep-sea microorganism. The cellularity was mimicked via Voronoi tessellation in the structure of the pavilion, whose structural performance was evaluated using finite element analysis. Accordingly, funicular structure design strategies were studied with a focus on cellular distributions and concentration responding to areas with high structural stress. The computer aided custom designed pavilion was constructed with engineered, in-house fabricated fiberglass composite materials. The bending-active lightweight structure was also validated through material performance inquiry, a partial full-scale cellular assembly, and the full-size pavilion construction. This work contributes to the design approach comprising a bending-active form-finding schematic strategy to construct the elastic bending-active structure physically and simulate computationally within the context of nature inspired innovative lightweight structure design.

Keywords Biomimetic design · Double-curved shell pavilion · Voronoi tessellation · Bending-active structures · Finite element analysis

1 Introduction

Bio-inspired architectural designs are getting nowadays, not only for novelty in design but for their structural performance. It is essential to comprehend the design of a biological structure, whose forms often seem complex but delicately balanced among geometry, material properties, and interacting forces. Within this context, the natural cellular structuring of Radiolaria, a unicellular microorganism, found in the oceans was considered in this work to design and construct a pavilion—a bending-active structure.

The bending-active structures, exhibiting complex curved shapes originated from flat elements [1–4], can demonstrate the relationship between form and structure. Such structures are advantageous, because they utilize systematic elastic deformations [5] as a form-defining and self-stabilizing strategy [6]. The Bend9 Structure [2] is one of the well-balanced examples that utilizing flat bent element to create a globally stable double curved form. The bending-active structures have the potential of integrating heterogeneity in its structure associated with a wide variety of design approaches [1, 6] and assembly methods, considering the constituent components and systems [7, 8]. Therefore, a healthy interdependent analogy between architectural (geometric) form and engineered structure is often observed in the bending-active structures. Additionally, the integration between the form and the structure is frequently achieved and simulated via Computer-Aided Design (CAD) partnered with structural analysis [9], form-finding (i.e., equilibrium force of a form) design [10–12] and more. A geometry created by such

✉ Tanvir R. Faisal
tanvir.faisal@louisiana.edu

[1] School of Architecture and Design, University of Louisiana at Lafayette, Lafayette, LA 70503, USA

[2] Department of Mechanical Engineering, University of Louisiana at Lafayette, Lafayette, LA 70503, USA

Published online: 07 February 2022

processes may offer a superior balance between structural performance and aesthetics.

Bending-active structures can be categorized into several structural typologies including actively bending plate [13], actively bending membrane, hybrids comprising membranes with elastically bent battens [14], and elastic kinetic members like cable and arches [6, 8]. These bending-active structural typologies can generate desired geometries that obtain the balance between form and stress equilibrium state. Three design approaches such as material behavior-based [13], geometry-based [15], and integral-based [1] are broadly considered when designing a bending-active structure. The advantages and deficiency of the bending-active structures were distinguished in the prior works by Lienhard [1], Riccardo [2], Schleichaer [11], and Sonntag [16]. The material behavior-based design approach relies upon material properties [17] to shape the structure and determine its performance. The geometry-based approach largely relies on structural geometry including cross-sections of the designed structure to meet the criteria within the allowable stress [18]. Finally, the integral approach tries to balance the material and geometry using computational tools.

A bending-active structure is often fabricated and erected using multiple single-curved elements to achieve a globally stable double-curved structure. To design a bending-active structure, it requires a strategy to utilize bending geometry and materials to meet the stiffness characteristic. The double-curved shell structures are advantageous over the single-curved geometry due to its ability to carry more compressive loads, such as a parabolic shell that can carry a uniform vertical load per unit on a horizontal axis [19]. Additionally, the bending-active structures are often confined with geometrical discontinuities, which require mechanical fastening for assembly during the construction where stresses are often concentrated on the mechanical fastening that reduces its global structural capacity. Designers and researchers around the globe have experimented with biomimetic approach in the design to reduce the stress on the mechanical fastening of bending-active structures. The biomimetic approach is to synthesize and learn from targeted species (Radiolaria herein) of its own survival essence and wisdom.

A group of multidisciplinary members from the Institute for Computational Design (ICD) and the Institute of Building Structures and Structural Design (ITKE) of the University of Stuttgart utilized a biomimetic approach to create a bottom-up pavilion design strategy, which was reflected in the 2015–16 ICD-ITKE Research Pavilion [16]. The design of the pavilion's internal module structure was inspired by the geometric morphology of a double-layered system of Echinoidea (Sea Urchin) and Clypeasteroida (Sand Dollar). Based on the two chosen species' biological principles and material characteristics, the pavilion material system was developed as a double-layered structure similar to the secondary growth in Sand Dollars. The internal module structure connections used finger joints and wood sewing technology to stitch the edges together. The pavilion design took the advantage of combining CAD and structural analysis to ensure structural integrity, and the multidisciplinary research group successfully demonstrated a geometry-based biomimetic design strategy as observed in ICD-ITKE Research Pavilion.

This research presents a detailed approach of taking the advantage of the geometry-based design strategy to construct an ultra-lightweight bending-active double-curved shell structure that utilizes biomimetic design approaches to create globally stable structures, focusing on the inclusiveness of CAD with structural analysis. The initial geometry studies of the Radiolaria pavilion include purple cone spruce [20], the cap of Morchella mushroom [21], and the structural features of Radiolaria [22]. After the initial screening, *Amphisphaera kina* Hollis [24]—one of the Radiolaria species—was selected for its morphological potential to meet the design criteria. Radiolaria's siliceous skeletons and the connected arrays of organic tubular struts often form a great variety of multi-vertex-based cellular structures [25] (similar to Voronoi diagram). However, the design of the proposed structure had a dimensional restriction, which forced us to obey a maximum boundary dimension of $2.60 \times 2.60 \times 2.80$ (h) meters. The feasibility of the bio-inspired architecture design was primarily explored and constructed in the "Competition and Exhibition of Innovative Lightweight Structures" organized in 2019 by the IASS Working Group 21 "Advanced Manufacturing and Materials" [26].

This paper is organized as follows. Section 2 illustrates the Radiolaria pavilion design concept and morphology. Section 3 describes the investigation of pavilion material and its mechanical characterization. Section 4 delineates the adopted design strategy coupled with CAD and structural analysis and its validation via a real-scale physical prototype, and Sect. 5 describes the final digital fabrication and the assembly of the pavilion. Finally, the major limitations and challenges are discussed in Sect. 6.

2 Design Concept of Radiolaria Pavilion via Voronoi Tessellations

The design of the Radiolaria pavilion was conceptualized based on the structural attributes of Radiolaria, which shrink its multi-vertex cellular structure (i.e., Voronoi structure) to withstand the flow forces by controlling the diameters of the bubbles. A massive cluster formed with many small bubbles has a large membrane surface, which finally results in a denser skeleton structure [26]. A similar structural morphology is often observed in many naturally evolved cellular structures, where the few-edged cell tends to be in

contact with many-edged cells and vice versa [28, 28, 30]. The graded cellularity of the skeletal structure relates its structural integrity to withstand stress either owing to self-weight or external forces. Radiolarians naturally optimize the graded multi-vertex cellularity and skeletal structure to resist applied loads.

A Radiolaria structure is primarily constructed with an inner endoplasm and an outer ectoplasm, including an organic bar in the center of the spine [30]. Furthermore, depending on locations, Radiolaria may have different forms of skeletal geometry in terms of the scales of pores and spines. The variation is natural and biomechanically regulated since the Radiolaria skeletal structure provides stability, while it floats in unobstructed seawater. Three key biomorphic features and principles of Radiolaria were discovered in the morphological analysis including the rib formation, pore size variation, and inner and outer surface development (Fig. 1). These principles play an essential role in the global stability of Radiolaria and were adopted in designing the Radiolaria inspired pavilion along with the features of Voronoi diagram.

To mimic the radiolarians' natural multi-vertex cellular structure in digital (CAD) modeling, we exploited Voronoi diagram function [30, 32], which divides the space into subspaces in an organic way as the core process of tessellation for the pavilion structure. Such technique has been applied in numerous fields including biology, metallurgy, crystallography, forestry, ecology, geology, geography, computer science, engineering [32–35], architectural installations, and facade morphologies [36–39]. A Voronoi diagram is mainly built on a set of points called Voronoi seeds where the multi-vertex cellular partitions are drawn based on a d-dimensional space into d-dimensional polyhedral cells based on the Euclidean distance between the seeds.

In this work, the research team opted to include radiolarian multi-vertex structural principle and the three morphology features in the bioinspired design. Additionally, three structural prerequisites emerged during the design investigation. First, the pavilion must be made out of modules to ease construction difficulty. Second, the pavilion must have self-supporting structural characteristics. Last, the pavilion material is capable of withholding stress while bending. Thus, it necessitates the materials investigation.

3 Materials

3.1 Materials Investigation, Selection, and Fabrication

A number of bendable materials [40, 40] was considered during the initial material investigation phase, including recycled High Density Polyethylene (HDPE) plastic, willow glass, and fiber-reinforced composite sheet. However, only recycled HDPE plastic and fiber-reinforced composite sheets have the potential to support the three structural prerequisites mentioned earlier in Sect. 2. The fiber-reinforced composite sheet was chosen due to the material's elasticity that can be controlled via material study and in-house fiber-reinforced composite sheet fabrication.

Two types of raw fiber-reinforced composites, Woven Roving (WR), and Chopped Strand Mat (CSM), were studied and coated with different thickness of high-strength polyester resin Bondo® mixtures. It was found that the variations of resin thickness affected the material's elastic performance. The WR fiber sheet samples exhibited the highest elastic performance (Fig. 2) compared with CSM samples (Fig. 3). Four out of five WR fiber sheet samples coated with different layers that can bend beyond a 50 mm radius with the thinnest WR fiber sheet made with only 0.9 g of high-strength polyester resin per 645.16 mm^2. To increase the WR fiber sheet thickness, a layering method was required due to the initial WR fiber sheet absorbability of the raw fiber. However, the WR raw fiber exhibits anisotropic bending behavior along the axial direction of the woven pattern, and thereby restricting the usage of WR raw fiber for structural reinforcement. The 3/4 oz CSM (weight ≈ 230 gm per sq. meter) has a random fiber

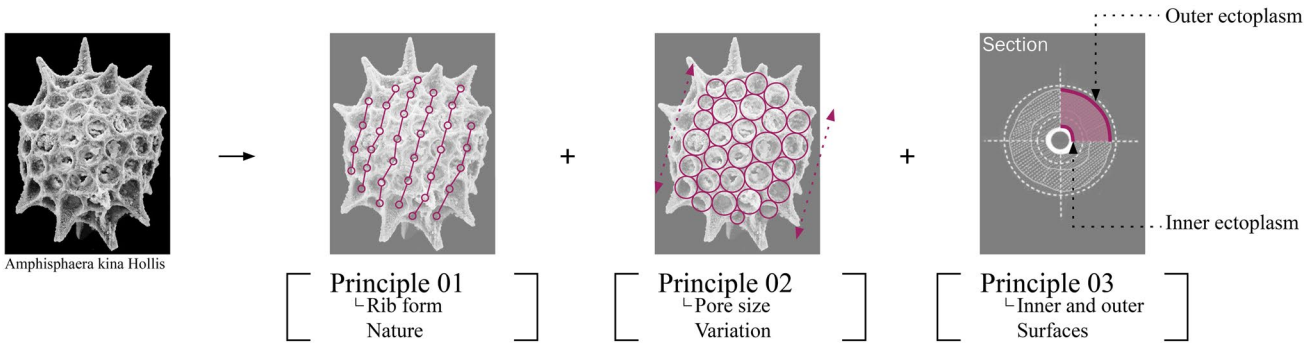

Fig. 1 Radiolaria biomorphic features

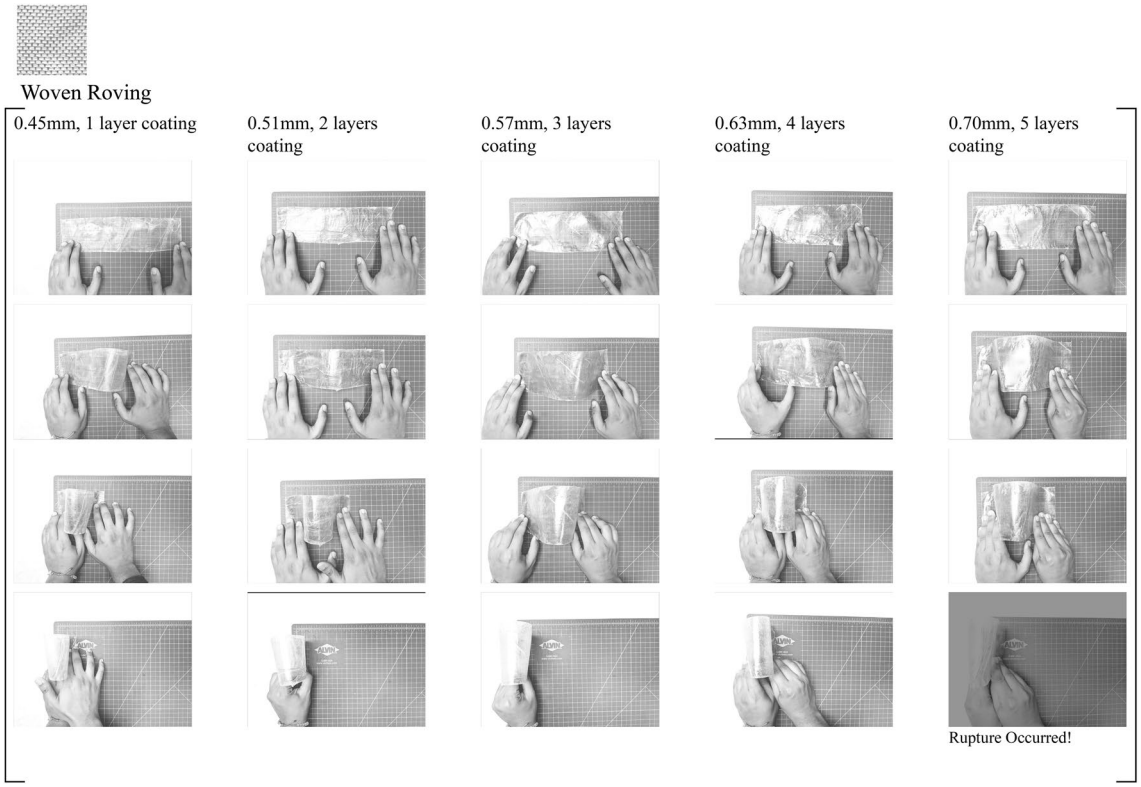

Fig. 2 Rupture test of the in-house fabricated Woven Roving fiberglass-reinforced composite (sheet) materials

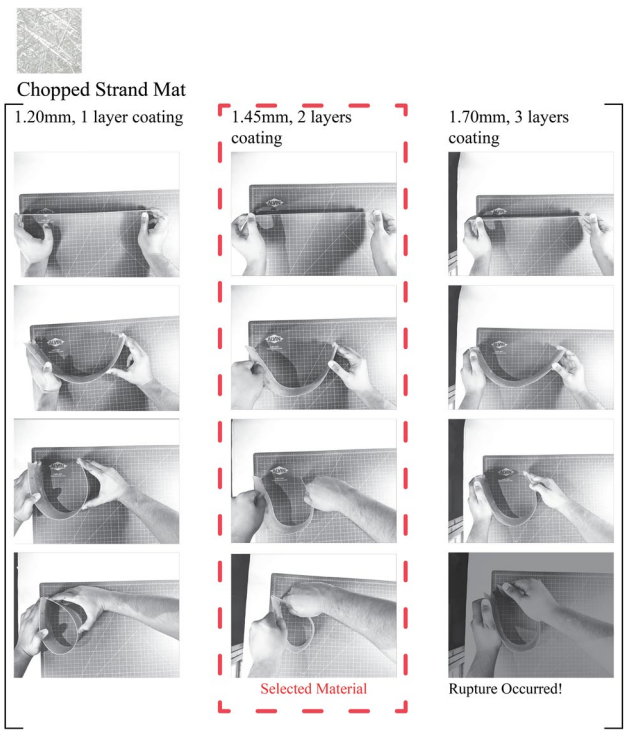

Fig. 3 Rupture test of the in-house fabricated Chopped Strand Mat fiberglass-reinforced composite (sheet) materials

orientation, which results in an isotropic bending behavior. Unlike WR raw fiber, CSM absorbs three times more (2.52 g per 645.16 mm^2) high-strength polyester resin. While the thickness of the fiber-reinforced composite sheet increased, it reduced the elastic performance concomitantly (Fig. 3). In Fig. 3, two out of three CSM samples can be bent to a 102 mm diameter circular shape without yielding to permanent deformation. The two layers of coating was chosen for its stiffness when it was bent to 102 mm diameter circular shape.

Several distinct features of fiber-reinforced composite sheet were also unveiled during the in-house fiber-reinforced composite sheet fabrication process. First, WR fibers could only absorb 0.21 g of high-strength polyester resin per 645.16 mm^2 after the first layer of coating. Second, building up to a predetermined thickness, the fabrication time for WR sheet drastically increased as coating process required 15-min time interval between each coating. Lastly, it was challenging to maintain a consistent thickness for the WR sheets due to the inconsistent absorption of the coated surface. In contrast, CSM exhibited a higher initial absorption capacity that helped with the uniform thickness. As a result, the materials investigation concluded with the fact that the CSM has better fabrication workability and exhibited isotropic bending behavior along with the elastic deformation behavior demonstrated by the initial qualitative rupture test.

3.2 Material Properties of CSM Fiber Sheets

A series of random 13 locations out of 8 CSM sheets were considered with an average thickness of 1.59 ± 0.03 mm. Meanwhile, 12 rectangular strips of 25 mm in width and 250 mm in length were randomly selected from different location and orientations and cut by a waterjet to conduct the uniaxial tensile tests to determine Young's modulus. The uniaxial tensile tests were performed as per the ASTM D3039 [41] in an MTS universal testing machine with a 100 kN load cell (Fig. 4a). Figure 4b shows the average stress–strain plot with standard deviations of the test specimens. The modulus was calculated as 6.1 (± 0.73) GPa.

4 Design of the Radiolaria Pavilion

4.1 Design of Initial Structure Based on Radiolarian Global Morphology

Different form-making shell geometries were investigated prior to the design of the final perimeter curve form-finding process (Figs. 5a–f). The investigation of geometries was to seek out the ideal aesthetic geometry, satisfying structural constraints, and spatial occupation requirements. The initial design study used the number of structural anchor points/legs to categorize structural stability as part of the evaluation. In theory, a structure with more legs offers better stability and stress distribution, but it often increases the construction difficulty based on the base's leveling and stability on each anchor point/leg. Therefore, the three-legged geometry was selected based on the self-leveling support characteristics, which eventually increased the structure's global stabilization.

Once a desirable outcome was reached in the initial form-making investigation, the digital modeling logic of the desirable geometry was interpreted. To generate Radiolarian cellular structure, it requires outer and inner surfaces. The pavilion's outer and inner surfaces (Fig. 5b, c) were created using Kiwi 3D isogeometric analysis software in Rhinoceros 3D. The outer perimeter started at a 1.3 m radius circle. It was divided into six equal parts to establish the anchor points for the legs and the crown headers. The outer and inner surfaces bending behavior mimics stiff rope-like behavior to simulate the catenary deformation (Fig. 5d, e). The final surfaces (Fig. 5f) were ready for the final cellular transformation.

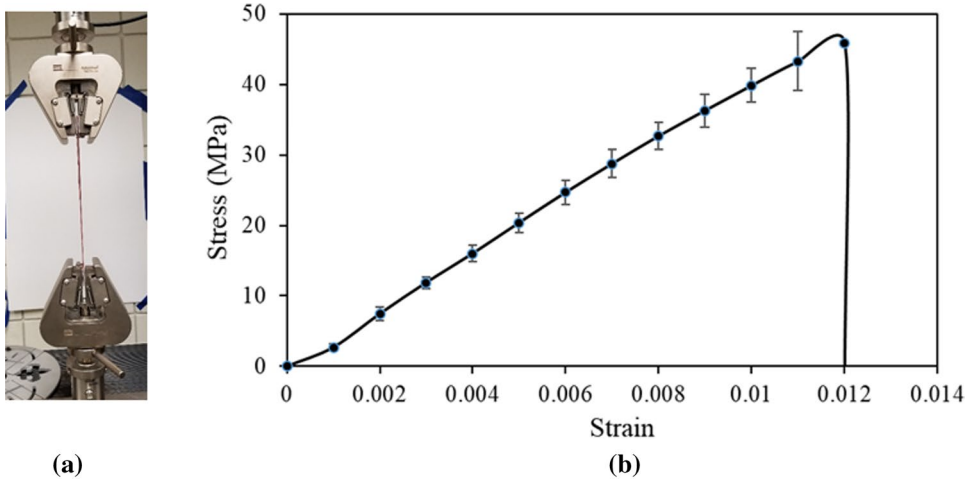

Fig. 4 Determination of materials properties of in-house fabricated fiberglass **a** uniaxial tensile test of a fiberglass strip as per ASTM D3039 and **b** average stress–strain plot with standard deviations of 12 test strips

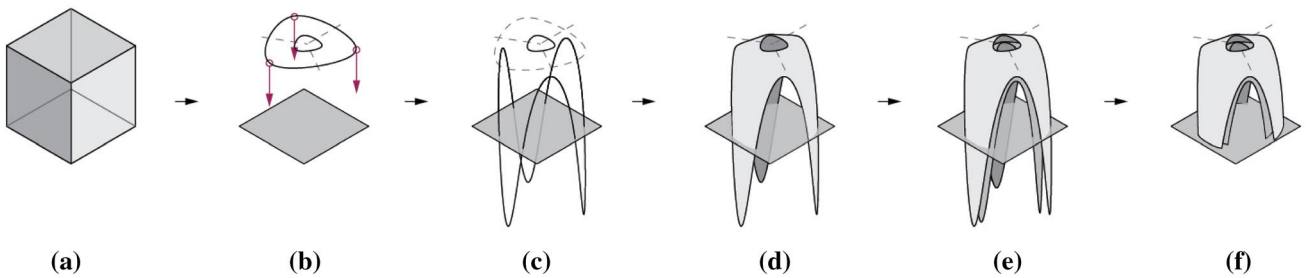

Fig. 5 Radiolaria pavilion form finding process

4.2 Structural Analysis of Initial Geometry via FEA

The advantage of the form-found perimeter curve allows force-driven-found geometries to act under compressive load. Thus, the geometry evaluation workflow was performed via FEA to ensure that the ultimate form is susceptible to compressive load. In the FEA, the structural analysis considered Dirichlet boundary conditions, i.e., imposing constraints. Since the pavilion under any circumstance should resist any ground-level displacement, we imposed constraint on the 6 degrees of freedom such that the three legs of the pavilion were completely fixed from displacements and rotations in the 3D space, i.e., $u_x = u_y = u_z = 0$ and $\omega_x = \omega_y = \omega_z = 0$, where u and ω denote displacement and rotation, respectively (Fig. 6). The material performance data, obtained experimentally in Sect. 3.2, was implemented in the initial form-finding design process and FEA investigation herein, considering only gravity load based on the assumption that the pavilion would be installed in an indoor environment. An approximate weight of 45 kg was primarily responsible for the gravity load. The outcomes of this design process can be marked as one of the baselines procedures for biomimetic design projects.

The objective of structural analysis of the initial geometry was to find the location of maximum stress, which is shown in von Mises stress distribution obtained via FEA (Fig. 6). Based on the findings, graded Voronoi tessellation was implemented by governing the Voronoi seeds distributions and cell sizes relating to the stress distributions.

4.3 Design of Voronoi Cell Mimicking Radiolarian Cell Morphology

In this study, the implementation of the grasshopper script created a flexible workflow (Fig. 8) that instantly correlated the structure geometry with Voronoi seeds, and the digital construction of the Radiolaria cellular structure. Cellular structuring was created with the Voronoi cells on both outer and inner shell surfaces (Fig. 7a, b) to mimic the radiolarian construction. The nodes on each cell were connected through interpolated curves (Fig. 7c) and thereafter extruded into the opposite direction of the cell normal plane (Fig. 7d). The same procedure repeated for the opposite cell which created intersect cone geometries that will create column-like structure as it aggregates. Subsequently, a Boolean subtraction was implemented to truncate the overlapping areas (Fig. 7e) and resulted in the radiolarian-like structure.

The load analysis of the initial pavilion structure via FEA (Sect. 4.2), and the materials properties of fiber composite material (Sect. 3.2) played a determinant role that influenced the distances and distribution pattern of the Voronoi seeds on the Radiolaria pavilion surfaces. First, the Voronoi seeds were equally distributed along the intersection of isocurves. The Voronoi seeds were generated by taking advantage of NURBS surface calculation and the directions of U and V (Fig. 8b, c), which allowed a surface isocurve to be extracted in the U or V direction. Each Voronoi seed is created from the intersection of U and V isocurves. One of the advantages of utilizing the extracting isocurve method in this study is the Voronoi seeds following the principal treeline (i.e., a rib-like or spine-like) that may facilitate load transfer mechanism from top to bottom of the structure. However, this method not necessarily guarantees a principal stress line outcome, but it highly depends on the creation process of the NURBS surface. In addition to the isocurve method, some manual points were also added to the lower section of the legs as surplus reinforcement to withstand the higher structural loads (Fig. 8d). The outcome of the primary design process (Sect. 4.2) basically establishes a dialogue between the design and structure that creates a foundation for generating the Voronoi cell distributions (Fig. 8e).

The Voronoi seeds pattern was eventually evolved and redistributed to reflect the outcome of the initial structural analysis. Hence, the densely populated Voronoi seeds were

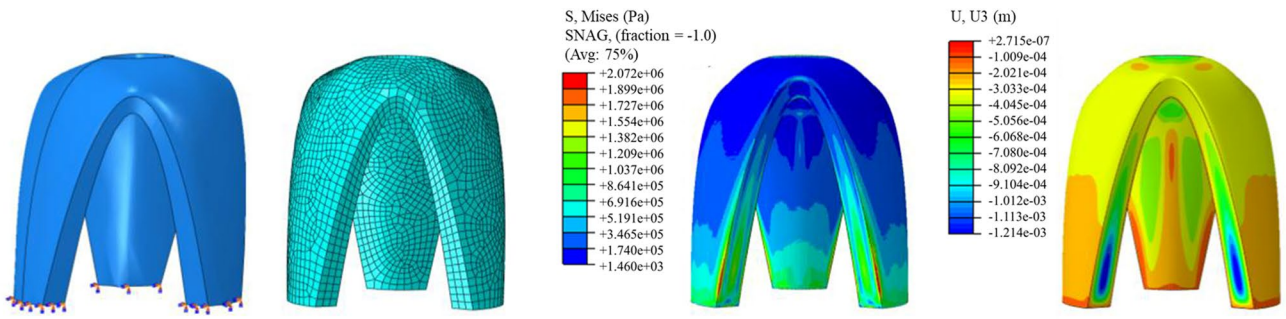

Fig. 6 FEA of primary CAD model showing BC (**a**), meshed model (**b**), and von Mises stress (Pa) (**c**) and deformation along the vertical direction (m) (**d**) due to gravity load

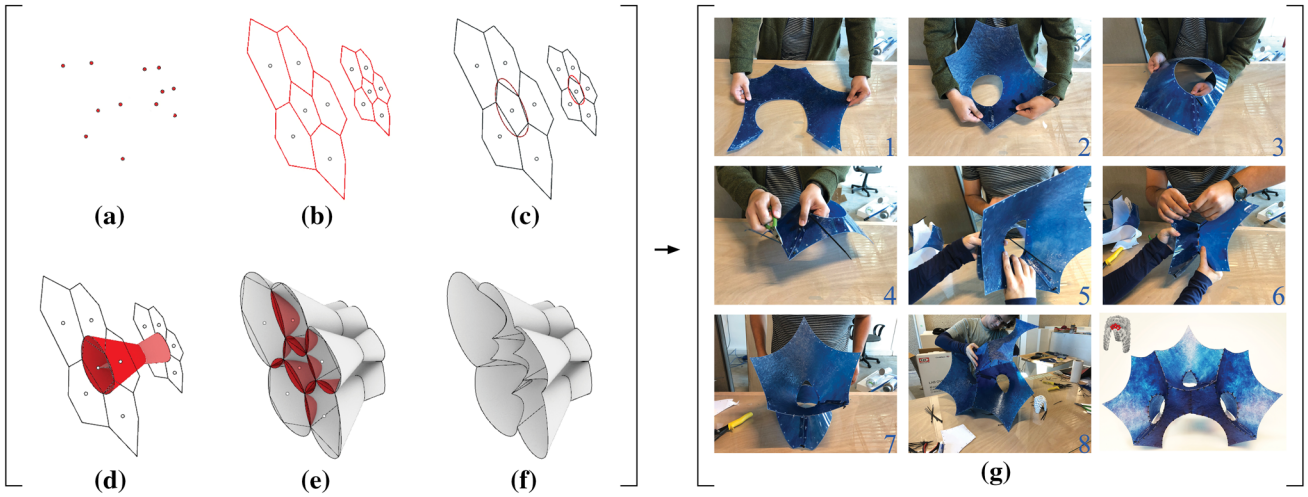

Fig. 7 Radiolarian digital creation procedure (Left) and physical model validation (Right)

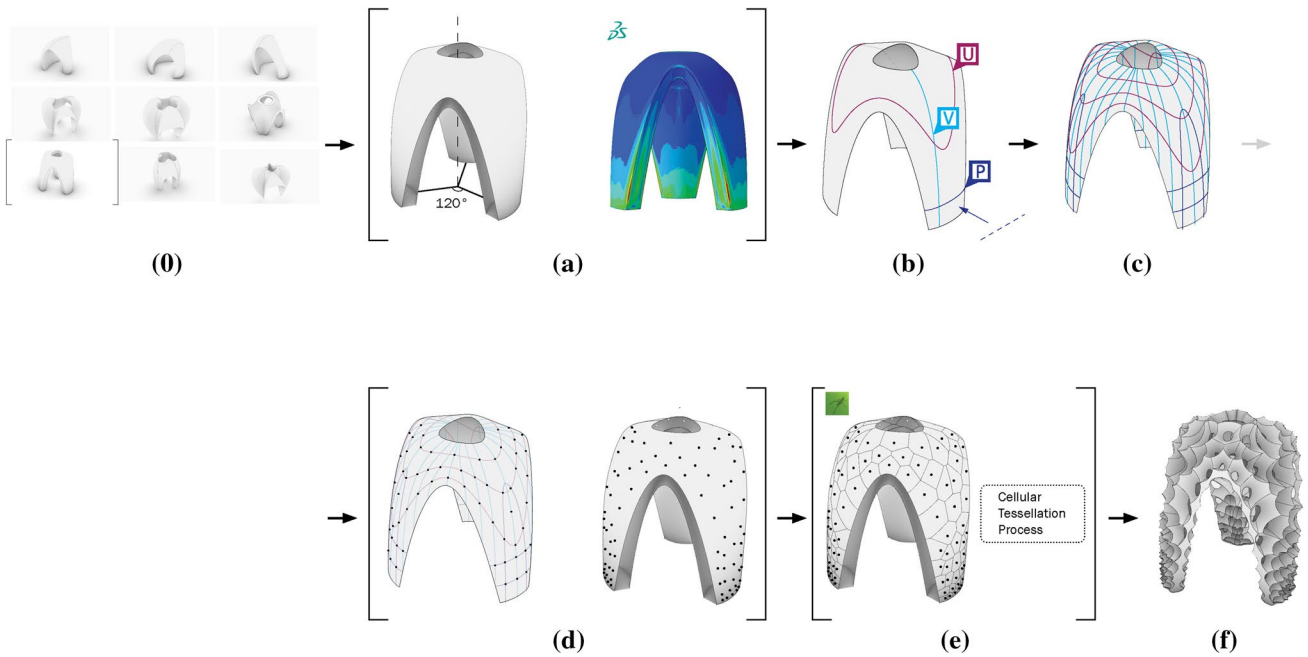

Fig. 8 Computational cellular tessellation process: form generation (**a**), surface curve extractions (**b**), surface curve population (**c**), control points generation (**d**), Voronoi cell tessellation (**e**), and finally the cellular pavilion (**f**)

0.2 m apart in the lower part of the pavilion, where the higher stress was observed, and the Voronoi seeds gradually spread out with greater distances, reflecting the lesser stress areas [38, 39]. Therefore, the ultimate Voronoi seeds pattern reflected the FE outcomes, respecting the fiber material bending limitations ranging from 0.2 to 0.76 m of bending diameter.

This digital design process was validated through a real-scale physical prototype (Fig. 6), while examining the rolling assembly process. Each Voronoi cell surface was designed with a pocket and a key (Fig. 9a) to assist the assembly joint (Fig. 9b), which was ultimately secured with high-performance cable ties. The process was repeatedly applied to connect with the neighboring cells (Fig. 7g) and result in a rolling assembly cellular structure. Evidently, the physical prototype demonstrated several key advantages by mimicking the morphology of the Radiolaria structure. This also offers a minimum storage requirement when it is unrolled, providing a fast and simple assembly process.

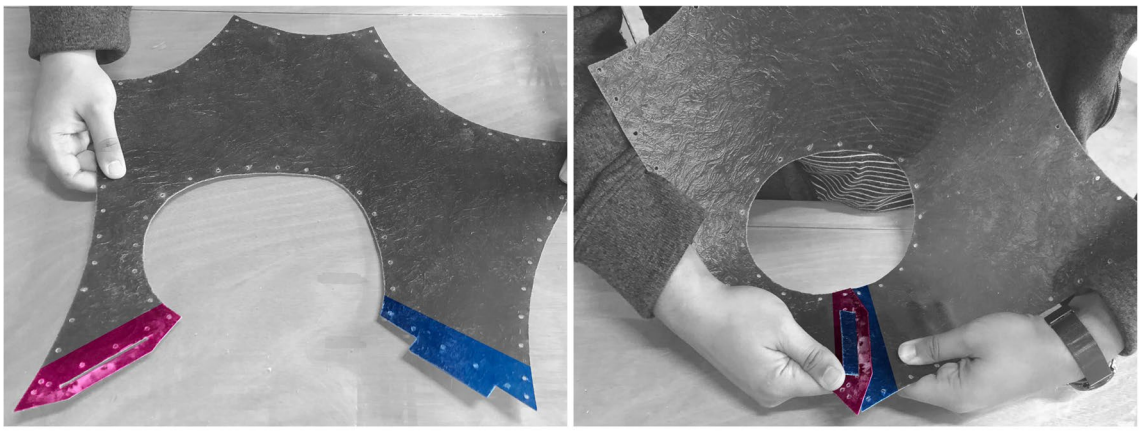

Fig. 9 Radiolarian cell pocket (red) and key (blue) joint (**a**), and joint connected (**b**)

4.4 FE Simulation and Post Design Analysis

For the detailed deformation and stress verification of the Radiolaria pavilion (with Voronoi cell structuring), the Radiolaria pavilion in.STEP format, preserving all the details of the CAD models, was exported to Abaqus for the FE analysis. A linear elastic isotropic material model was considered based on the in-house fabricated fiberglass composites and its materials properties determined as described in Sect. 3.2. The verification was conducted for the overall behavior such as the stress distributions of the pavilion under gravity load since the pavilion was designed as well as installed in an environment without any wind load. The model was meshed with three-dimensional shell element S4, a 4-node, quadrilateral doubly curved general-purpose shell element with finite membrane strain (Fig. 10). The mesh was refined unless we achieved a 5% variation of the maximum von Mises stress between the two consecutive simulations. A similar boundary condition that is completely fixed from displacements and rotations was applied. During the FEA, pre-stress in the individual cell's shell structure due to bending has been considered. An equi-biaxial initial stress condition equal to 5% of the initial yield stress is prescribed for the shell elements in step-1 (initial conditions). The initial step allows us to implement prestress (predefined field) that is applicable at the very beginning of the analysis. However, the prestress was not held constant in the analysis steps and allowed to change to accommodate additional deformation in the cells. If the prestress is not held constant in analysis steps following the step in which it is held constant, the stress in the composite sheet will change due to additional deformation in the cell. If there is no additional deformation,

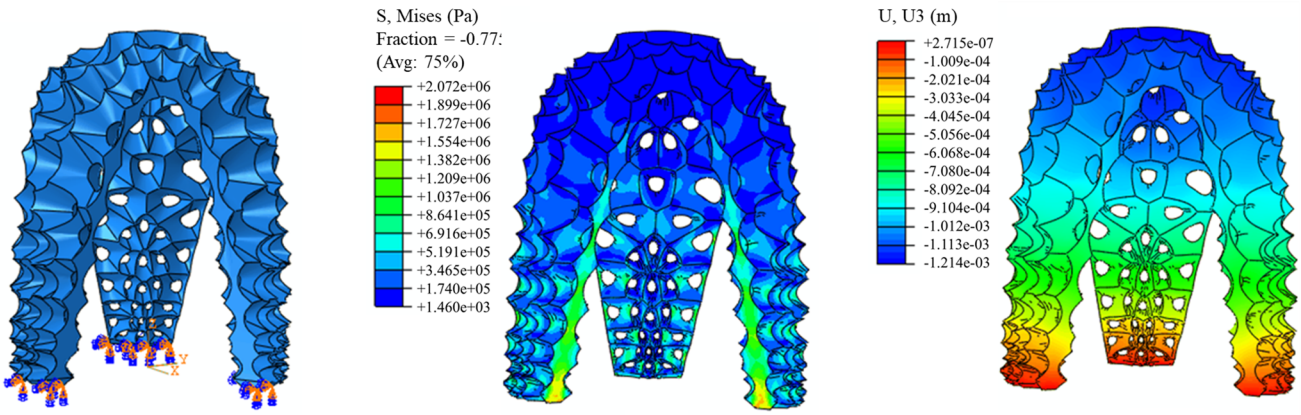

Fig. 10 FEA of the final CAD model of Radiolaria pavilion with cellular structuring showing BC (**a**), von Mises stress (Pa) (**b**), and deformation along the vertical direction (m) (**c**) due to gravity load

the stress will remain at the level set by the initial conditions. In this FEA, we considered two limiting assumptions. First, the simulation was conducted with a CAD model, where the cell edges were continuously and perfectly connected to each other, but in the actual pavilion, cable ties were used for the edge-to-edge connection. Since high strength cable ties were used and very tightly attached, the displacement as well as shear stress between the edges were minimized and reasonably satisfied the assumption. Next, a uniform prestress has been considered throughout, ignoring the differences in shapes between the Voronoi cells, a limiting assumption in the FEA. However, the FE simulation verified that the graded cellularity strengthened the structure at the lower region of the pavilion (Sect. 4.3 model), and thereby preventing the local deformation observed in the FEA of the model (Fig. 6d).

5 Fabrication and Assembly of the Pavilion

Prior to the fabrication, each cell was digitally unrolled from the cellular-cone-like geometry into a flat surface. Each cell was given a custom-designed labeling system (Fig. 11a) to indicate its location, the top indicator (number of sections), the mid indicator (outer or inner cell), the bottom indicator (number location within a section). The cells in each section were organized in a linear order to avoid potential onsite assembly difficulties. The main reason for utilizing a circular shape in the indication system was to minimize the structural damage on the fiber composite surface from the fabrication cut-out and to avert the surface anisotropic bending due to the cut-out modification. Since the pavilion design was composed of three identical sections, it was not required to differentiate leg numbers in the labeling system.

It was advantageous to have identical sections because the symmetry drastically reduced the waterjet fabrication time. Each cell had been cut on three sheets of fiberglass composite material that were temporarily sandwiched together, a cut-on-cut fabrication technique. Several weights were used to secure the position of the sheets (Fig. 11b). This process is adopted due to the structural resistance of the fiberglass sheet that prevents itself from shattering because of initial waterjet contact with the material. Adversely, one disadvantage is a slower cutting speed because of the weights on the sheet material. The waterjet head would often closely run into the weights that required the supervising members to pay close attention and paused the waterjet cutting process to relocate the weights ahead of the cut path. Still, this fabrication methodology significantly reduced the fabrication time to one-third (i.e., from the estimated 60 to 20 h).

The final construction (Fig. 12a–d) was similar to the prototype assembly process (Fig. 7g), which utilized high-performance cable ties to join the side of the neighboring cells by forming a unity structure. Following the pavilion design, the assembly sequence started from the bottom and capped it off with the top section. The total hours of the construction process took nearly 10 h, with an average of a group of three people to complete. As a result, the Radiolaria pavilion (i.e., real scale prototype) proves its ability to support itself without noticeable visual deviation such as misalignment in the overall structure. However, a few areas with higher stress did break off at the connection points (Fig. 13a) and had minor buckling (Fig. 13b). It is beyond the scope of current work, whether the issue relates to high-stress concentration or the waterjet cutting process weakening the area or mis-shape in the material making process. At the end, the Radiolaria pavilion construction validated the three Radiolaria morphology features in design and the structural prerequisites, which

Fig. 11 Labeling system of assembly (**a**), and fabrication process (**b**) in waterjet cutting process

(a) (b) (c) (d)

Fig. 12 Assembly process of the Radiolaria pavilion

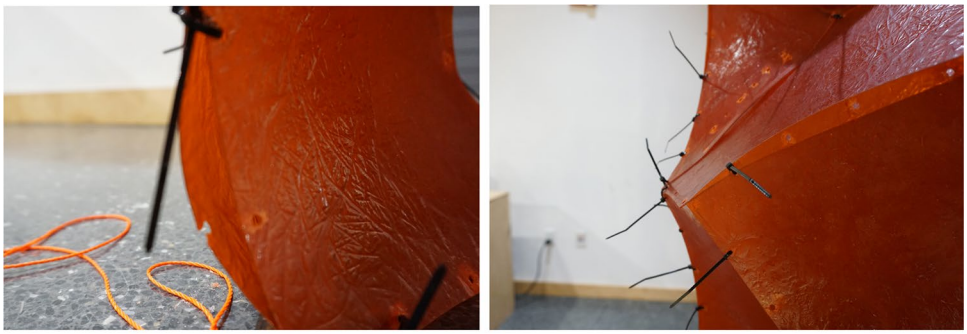

(a) (b)

Fig. 13 Local failure (break off) (**a**), and local buckling of the fiberglass material (**b**)

encompass modular construction and self-supporting structure, and the material's ability to support stress.

6 Limitation and Challenges on Design and Fabrication

Despite many advantages, there were challenges associated with the design and construction method. Design challenge is related to the separate entities of computational CAD modeling software (i.e., Rhinoceros 3D) and the FEA software (i.e., Abaqus) that restricted the direct data streaming in the design process. As a result, the design reflected the FEA outcome was achieved linearly after the pavilion geometry was form-found although the form-found geometries should have compression characteristics. During the form-finding process, the geometries are using rope character as the simulation material; therefore, the final 3D geometries might not be the most optimized version. Due to this limitation, the form-found geometry to the FEA iteration process is processed only once. Furthermore, FEA was conducted with a few limiting or simplifying assumptions (mentioned in Sect. 4.4), which ignored more complex stress distribution within the pavilion structure. Therefore, it is fair to say that there might be other possible optimum outcomes than this final pavilion form-found geometry.

Another major challenge in this work, besides the time limitation, was to simulate the dynamic bending scheme computationally with the essential constituents through dynamic relaxation programming or achieved via FE solver/software. In some cases, researchers deploy custom programming solutions that integrate with the design process, particularly with the projects that utilize custom-engineered materials. In this work, material bending limitation data was translated via the form of Voronoi seeds distances and patterns that were embedded within the computational parameters to tessellate the structure and to avoid the material of the structure being overloaded with stress. Due to the material's structural performance and cell connection, the global form reacted to a limited lateral force. Yet, the relationship between the material bending limitation data and the Voronoi seeds distances do not have direct parametric relationship for optimization. As a result, the final Voronoi seeds distances were manually adjusted.

The global stability of the structure heavily relied on the edge-to-edge fasteners. The stress distribution on these fasteners is an essential part of the design; otherwise, it will risk localized failure. The edge-to-edge joint of the Radiolaria pavilion offers greater flexibility in the assembly process. However, the current fastener joint system cannot withhold other than the pavilion's self-weight. Therefore, an alternative edge-to-edge connection system must be considered for future research. Additionally, a global structural leveling evacuation was considered in the form-making shell geometries study, no structural analysis was performed on these geometries. The design of a three-legged structure is not apparently the most structurally sound decision, but the computational structural (FEA) analysis of the current geometry has substantiated it as a viable selection. Finally, a larger bending radius with a deeper cone shape has a higher chance of buckling and deforming at local and global states. Subsequently, the cell size has a minimum of 0.2 m with 0.35 m deep cone-shape and a maximum of 0.76 m bending radius with 0.2 m shallow cone-shape.

7 Conclusions

There are very few precedents in the field of bending active plate with rolling assembly through form-finding, e.g., Bend9 Structure by Riccardo [2]. Although the pavilion design apparently takes a few similar characteristics from Bend9, the Radiolaria pavilion is unique as it does not have either a substrate structural system to support the external surfaces or utilize plate on plate connection. The design approach, in this work, illustrated a bending-active form-finding schematic strategy to simulate the elastic bending-active structure physically and computationally, and the challenges of integrating the computational process. The current work investigated the engineered fiberglass composite plate elastic behavior that influenced the final pavilion structure build-up and its load deformation response. To strengthen the structure, the pavilion's design utilized the radiolarian biomorphic features combined with the Voronoi algorithm to form the bending shell structure. The developed construction system took advantage of the fiberglass composite strength and used the edge-to-edge connection with high-performance cable ties. This work contributes to the design approach comprising a bending-active form-finding schematic strategy to simulate the elastic bending-active structure physically and computationally within the context of nature inspired innovative lightweight structure design.

Acknowledgements The authors would like to thank the team of students who worked on this project: Quoc Dang, Jesse Heath, Sami Jaber, Son Nguyen, Catherine Reaux, Olivia Welty, and Professor Corey Saft, as well as the support of Dr. Charles Taylor, Dr. Jacob King and Yasmeen Qudsi on waterjet cutting. The authors acknowledge the support provided by the University of Louisiana at Lafayette, the College of the Arts, and by MAO.JIN.DAO Design.

Declarations

Conflict of interest The authors declare that there is no conflict of interest.

References

1. Lienhard, J., Alpermann, H., Gengnagel, C., & Knippers, J. (2013). Active bending, a review on structures where bending is used as a self-formation process. *International Journal of Space Structures, 28*, 187–196. https://doi.org/10.1260/0266-3511.28.3-4.187
2. Riccardo, L. M. (2017) *Bending-active plates: strategies for the induction of curvature through the means of elastic bending of plate-based structures.* Institut für Tragkonstruktionen und Konstruktives Entwerfen, Universität Stuttgart, Stuttgart, Germany. https://elib.uni-stuttgart.de/handle/11682/9406.
3. Panetta, J., Konaković-Luković, M., Isvoranu, F., Bouleau, E., & Pauly, M. (2019). X-shells: a new class of deployable beam structures. *ACM Transactions on Graphics, 38*(4), 1–15. https://doi.org/10.1145/3306346.3323040
4. Laccone, F., Malomo, L., Pietroni, N., Cignoni, P., & Schork, T. (2021). Integrated computational framework for the design and fabrication of bending-active structures made from flat sheet material. *Structures, 34*, 979–994. https://doi.org/10.1016/j.istruc.2021.08.004
5. Knippers, J., Cremers, J., Gabler, M., & Lienhard, J. (2012). *Construction manual for polymers+ membranes: materials, semi-finished products, form finding, design.* Birkhäuser GmbH, Munich, Germany
6. Lienhard, J. (2014). *Bending-active structures: form-finding strategies using elastic deformation in static and kinetic systems and the structural potentials therein*. Institut für Tragkonstruktionen und Konstruktives Entwerfen, Universität Stuttgart, Stuttgart, Germany. https://doi.org/10.18419/opus-107
7. Iwamoto, L. (2013). *Digital Fabrications: Architectural and Material Techniques*. Princeton Architectural Press.
8. Schleicher, S. (2018). Potential of 3D printed joinery for bending-active structures. Proceedings of IASS Annual Symposia, IASS 2018 Boston Symposium: Construction-aware Structural Design, Boston, USA, 1–6.
9. Schleicher, S., Rastetter, A., Riccardo, L. M., Schönbrunner, A., Haberbosch, N., & Knippers, J. (2015). Form-finding and design potentials of bending-active plate structures. In M. R. Thomsen, M. Tamke, C. Gengnagel, B. Faircloth, & F. Scheurer (Eds.), *Modelling Behaviour: Design Modelling Symposium* (pp. 53–63). Springer.
10. Riccardo, L. M., Schleicher, S., & Knippers, J. (2016). Bending-active plates: form and structure. *Advances in architectural geometry* (pp. 170–187), vdf Hochschulverlag AG, Zurich, Switzerland.
11. Schleicher, S., & Riccardo, L. M. (2016). Bending-active plates: form-finding and form-conversion. https://ced.berkeley.edu/research/faculty-projects/bending-active-plates-form-finding-and-form-conversion.

12. Laccone, F., Malomo, L., Pérez, J., Pietroni, N., Ponchio, F., Bickel, B., & Cignoni, P. (2020). A bending-active twisted-arch plywood structure: Computational design and fabrication of the FlexMaps Pavilion. *SN Applied Sciences, 2*(9), 1–9. https://doi.org/10.1007/s42452-020-03305-w
13. Riccrdo, L. M., & Knippers, J. (2017). On the behaviour of bending-active plate structures. Proceedings of the IASS Annual Symposium 2017 "Interfaces: architecture, engineering, science, 2017 Hamburg, Germany, 1–9.
14. Riccardo, L. M., Fragkia, V., Längst, P., Lienhard, J., Noël, R., Šinke Baranovskaya, Y., Tamke, M., & Ramsgaard Thomsen, M. (2018). Isoropia: An encompassing approach for the design, analysis and form-finding of bending-active textile hybrids. Proceedings of IASS Annual Symposia, IASS 2018 Boston Symposium: Construction-aware Structural Design, Boston, USA, 1–8.
15. Brancart, S., Popovic L. O., De Laet, L., & De Temmerman, N. (2018). Bending-active reciprocal structures: geometric parameters and their stiffening effect. Proceedings of IASS Annual Symposia, IASS 2018 Boston Symposium: Construction-aware Structural Design, Boston, USA, 1–8.
16. Sonntag, D., Bechert, S., & Knippers, J. (2017). Biomimetic timber shells made of bending-active segments. *International Journal of Space Structures, 32*, 149–159.
17. Gengnagel, C., Hernández, E. L., & Bäumer, R. (2013). Natural-fibre-reinforced plastics in actively bent structures. *Proceedings of the Institution of Civil Engineers - Construction Materials, 166*(6), 365–377.
18. Bletzinger, K.-U., Firl, M., Linhard, J., & Wüchner, R. (2010). Optimal shapes of mechanically motivated surfaces. *Computer Methods in Applied Mechanics and Engineering, 199*, 324–333.
19. Adriaenssens, S., Block, P., Veenendaal, D., & Williams, C. (2014). *Shell structures for architecture: Form finding and optimization*. Routledge.
20. Harikumar, A., Bovolo, F., & Bruzzone, L. (2017). An internal crown geometric model for conifer species classification with high-density lidar data. *IEEE Transactions on Geoscience and Remote Sensing, 55*(5), 2924–2940. https://doi.org/10.1109/TGRS.2017.2656152
21. Larson, A. J., Cansler, C. A., Cowdery, S. G., Hiebert, S., Furniss, T. J., Swanson, M. E., & Lutz, J. A. (2016). Post-fire morel (Morchella) mushroom abundance, spatial structure, and harvest sustainability. *Forest Ecology and Management, 377*, 6–25.
22. Anderson, O. R. (2012). *Radiolaria*. Springer. https://doi.org/10.1007/978-1-4612-5536-9
23. Hollis, C. J. (1993). Latest cretaceous to late Paleocene radiolarian biostratigraphy: A new zonation from the New Zealand region. *Marine Micropaleontology, 21*(4), 295–327. https://doi.org/10.1007/s42452-020-03305-w
24. Morphocode. (2009). Radiolaria: microworld's architecture. https://morphocode.com/radiolaria-microworld-architecture/
25. Liu, B., Faisal, T., Saft, C. L., Heath, J., Jaber, S. A., Dang, Q., Reaux, C., Welty, O., & Nguyen, S. (2019). Lightweight cellular structure: A formless fiberglass buildup utilize bending-active. Proceedings of the IASS Annual Symposium 2019 – Structural Membranes 2019 Form and Force, Barcelona, Spain, 1–5.
26. Duthie, L. (2014). Radiolaria shell structure. https://blogs.ubc.ca/bionictimber/2014/03/01/radiolaria-shell-structure/
27. Chiu, S. (1995). Aboav-Weaire's and Lewis' laws—A review. *Materials characterization, 34*(2), 149–165. https://doi.org/10.1016/1044-5803(94)00081-U
28. Lewis, F. T. (1931). A comparison between the mosaic of polygons in a film of artificial emulsion and the pattern of simple epithelium in surface view (cucumber epidermis and human amnion). *The Anatomical Record, 50*(3), 235–265.
29. Faisal, T. R., Hristozov, N., Rey, A. D., Western, T. L., & Pasini, D. (2012). Experimental determination of *Philodendron melinonii* and *Arabidopsis thaliana* tissue microstructure and geometric modeling via finite-edge centroidal Voronoi tessellation. *Physical Review E, 86*(3), 031921. https://doi.org/10.1103/PhysRevE.86.031921
30. Radiolaria: Biology. https://doi.org/10.1007/s42452-020-03305-w.
31. Okabe, A., Boots, B., Sugihara, K., & Chiu, S. N. (2009). *Spatial tessellations: Concepts and applications of Voronoi diagrams*. John Wiley & Sons.
32. Blackman, J., & Mulheran, P. (1996). Scaling behavior in submonolayer film growth: A one-dimensional model. *Physical Review B, 54*(16), 11681. https://doi.org/10.1103/PhysRevB.54.11681
33. Faisal, T. R., Hristozov, N., Western, T. L., Rey, A. D., & Pasini, D. (2014). Computational study of the elastic properties of *Rheum rhabarbarum* tissues via surrogate models of tissue geometry. *Journal of Structural Biology, 185*(3), 285–294. https://doi.org/10.1016/j.jsb.2014.01.012
34. González, D. L., Pimpinelli, A., & Einstein, T. (2011). Spacing distribution functions for the one-dimensional point-island model with irreversible attachment. *Physical Review E, 84*(1), 011601. https://doi.org/10.1103/PhysRevE.84.011601
35. Clifford, B., & McGee, W. (2013). *Range: Matter Design*. Matter Design Press.
36. Zhao, B., Chen, W., Hu, J., Chen, J., Qiu, Z., Zhou, J., & Gao, C. (2016). Mechanical properties of ETFE foils in form-developing of inflated cushion through flat-patterning. *Construction and Building Materials, 111*, 580–589.
37. Angelucci, G., & Mollaioli, F. (2018). Voronoi-like grid systems for tall buildings. *Frontiers in Built Environment*. https://doi.org/10.1007/s42452-020-03305-w
38. Su, Y., Wu, Y., Ji, W., & Sun, X. (2021). Computational morphogenesis of free-form grid structures with Voronoi diagram. *Computer-Aided Civil and Infrastructure Engineering, 36*(3), 318–330. https://doi.org/10.1111/mice.12621
39. Froli, M., & Laccone, F. (2017). Experimental static and dynamic tests on a large-scale free-form Voronoi grid shell mock-up in comparison with finite-element method results. *International Journal of Advanced Structural Engineering, 9*(3), 293–308. https://doi.org/10.1007/s40091-017-0166-9
40. Pietroni, N., Tonelli, D., Puppo, E., Froli, M., Scopigno, R., & Cignoni, P. (2015). Statics aware grid shells. *Computer Graphics Forum, 34*(2), 627–641. https://doi.org/10.1111/cgf.12590
41. ASTM D3039 (2017), Standard test method for tensile properties of polymer matrix composite materials, ASTM International.

Publisher's Note Springer Nature remains neutral with regard to jurisdictional claims in published maps and institutional affiliations.